Production of ^{229}Th for medical applications: Excitation functions of low-energy protons on ^{232}Th targets

J. R. Griswold, C. U. Jost, D. W. Stracener, S. H. Bruffey, D. Denton, M. Garland, L. Heilbronn, and S. Mirzadeh

Phys. Rev. C **98**, 044607 — Published 12 October 2018

DOI: 10.1103/PhysRevC.98.044607

Production of ^{229}Th for medical applications: excitation functions of low-energy protons on ^{232}Th targets

J. R. Griswold,[1,3] C. U. Jost,[2,4] D. W. Stracener,[2] S. H. Bruffey,[1] D. Denton,[1]

M. Garland,[1*] L. Heilbronn,[3] and S. Mirzadeh[1]

Divisions of Nuclear Security and Isotope Technology,[1] and Physics,[2] Oak Ridge National Laboratory, Oak Ridge, TN 37831, USA.

Departments of Nuclear Engineering,[3] and Physics and Astronomy,[4] University of Tennessee, Knoxville, TN 37996, USA.

*Current address: Department of Energy, Office of Nuclear Physics, Isotope Program, SC-26/Germantown Building, 1000 Independence Ave., SW, Washington, DC 20585.

Key words: Thorium-229, protactinium-229, actinium-225, bismuth-213; proton-induced nuclear reaction, 25 MV tandem accelerator, targeted alpha therapy

ABSTRACT

As a part of a general program to evaluate production routes for ^{229}Th, we studied production of ^{229}Th via proton-induced reactions on ^{232}Th targets bombarded with low-energy protons, $E_p \leq$ 40 MeV. The reported excitation functions include those for proton-induced reactions on natural thorium yielding to $^{228, 229, 230 \& 232}$Pa isotopes; ^{232}Th(p,xn) reactions, where x = 1, 3, 4, and 5, at proton energy ranges of 12–40 MeV. Although the data for ^{232}Th(p,n)^{228}Pa, ^{232}Th(p,3n)^{230}Pa, and ^{232}Th(p,5n)^{232}Pa reactions were deduced by direct analysis of the thorium foils after irradiation, the data for ^{232}Th(p,4n)^{229}Pa were obtained by radiochemical techniques. The half-life of ^{229}Pa was evaluated and determined to be 1.55 ± 0.01 d. Further, the α-branching ratio, α/(α + EC) of ^{229}Pa was evaluated to be 0.53 ± 0.10% by allowing ^{229}Pa to decay for ~7 d, then chemically extracting and quantifying the ^{225}Ac ($t_{1/2}$ = 10.0 ± 0.1 d) from ^{229}Pa samples. In addition, we

report the effective production cross section of ^{229}Th in a thick ^{232}Th target in the proton energy range of 23–33 MeV. The peak of the excitation function for the ^{232}Th(p,4n)^{229}Pa reaction occurs at 162 ± 14 mb and E_p = 29.7 ± 0.5 MeV. This is only slightly larger than the effective cross section for the ^{232}Th(p,x)^{229}Th reaction (obtained from a thick target experiment). This data indicates that the ^{232}Th(p,4n)^{229}Pa reaction is the major reaction pathway for the cumulative ^{232}Th(p,x)^{229}Th reaction cross section in this energy range. The measured cross sections were compared with theoretical cross sections using the simulation codes Particle and Heavy Ion Transport code System (PHITS) and Monte Carlo Neutral Particle 6 (MCNP6). At proton energy ranges of 12–33 MeV, the cumulative excitation function predicted by PHITS for the reactions leading to ^{229}Th was in close agreement with the experimental function, whereas the function predicted by MCNP6 was a factor of two higher at the peak of the excitation function.

I. INTRODUCTION

Radioimmunotherapy using α-emitting radionuclides is a promising and rapidly expanding method for treating oncologic diseases. In recent years, it has been shown that transporting α-emitting radionuclides by biological carriers such as engineered peptides and antibodies to precise locations of tumor tissues or metastatic cells results in selective irradiation of targeted tissues with minimal damage to normal and non-target tissues. This is due to the high initial energy of α-particles (5–8 MeV from natural decay of α-emitting radioisotopes) and their short range in biological tissues (less than 100 μm, ~10 cell diameters), which allows for the deposition of high-level energy in the vicinity of decaying radionuclides [1]. Consequently, α-emitters are most suitable for the treatment of micro-metastases and have shown to be very effective for the treatment of blood cancers such as acute myeloid leukemia, and α-emitters appear promising in the treatment of micro-metastases in neoplastic diseases [2-4]. Of the approximately one million new cases of cancer (excluding non-melanoma skin cancer) that occur annually in the United States, about 33% already have metastasized, and about 67% initially appear to be a local disease. About 40% of these will subsequently develop distant metastases [5]. The subset of patients with micro-metastases may benefit from adjuvant α-therapy. Further, recent clinical trials have shown that relapsed cancer patients who have not responded to conventional chemotherapy can be treated using radiolabeled antibodies with extraordinary

success [6]. The potential applications of α-emitters for the treatment of other malignancies—such as skin, breast, prostate, and lung cancers—have also been demonstrated [7-10].

Among prospective α-emitters, ^{212}Bi ($t_{1/2}$ = 60.55 ± 0.06 min), ^{223}Ra ($t_{1/2}$ = 11.4 d),[11-13] ^{225}Ac ($t_{1/2}$ = 10.0 ± 0.1 d), and ^{211}At ($t_{1/2}$ = 7.214 ± 0.007 h) are of major interest [14,15]. However, considering the combined nuclear, physical, chemical and biological properties, ^{225}Ac and its daughter ^{213}Bi ($t_{1/2}$ = 45.61 ± 0.06 min) are of greatest interest [15-17]. Ongoing clinical trials with ^{213}Bi have demonstrated its efficacy in treatment of oncologic diseases. It is particularly important that the radionuclide ^{213}Bi can be used at early stages of treatment of many cancer types, as well as in combination with other methods (e.g., surgery, chemotherapy) [18]. A recent review of targeted alpha therapy is available [19].

Bismuth-213 and its precursor ^{225}Ac are the decay products of long-lived ^{229}Th ($t_{1/2}$ = 7932 ± 55 y) [20]. In turn, ^{229}Th is a decay product of ^{233}U [$t_{1/2}$ = (1.592 ± 0.002) x 10^5 y] and can be obtained from stockpiles of this very long-lived isotope of uranium [21,22]. The decay process starts with ^{233}U, which is the current production source of ^{229}Th, and continues through two generator systems involving four intermediate radioisotopes and finally results in ^{213}Bi, with a half-life of 45.6 min. The current annual supply of ^{225}Ac worldwide is about 1.7 Ci [23]. This quantity is insufficient to support existing clinical trials and laboratory investigations. Various clinical trials are impeded or suspended, and future research projects are not being initiated because of the lack of availability of ^{225}Ac.

A number of methods are currently being pursued for producing useful quantities of ^{229}Th and ^{225}Ac. Thorium-229 can be extracted from existing ^{233}U stockpiles [21] or produced by multiple and single neutron capture of ^{226}Ra and ^{228}Ra targets in a high-flux nuclear reactor through the ^{226}Ra(3n,2β)^{229}Th and ^{228}Ra(n,2β)^{229}Th reactions, respectively [22,24]. Alternatively, ^{225}Ac can be made directly utilizing the ^{226}Ra(p,2n)^{225}Ac or ^{226}Ra(γ,n) ^{225}Ra($t_{1/2}$ =14.9 ± 0.2 d, β^-)^{225}Ac reactions or by the spallation reaction of a ^{232}Th target with high energy protons [25-28]. Other projectiles such as alpha particles and deuterons incident on a ^{226}Ra target have also been suggested. [15]

As noted, the current supply of ^{229}Th (extracted from ^{233}U) is insufficient to support multiple clinical trials, and the safeguards associated with ^{233}U limits access to this valuable source [21]. The production of ^{229}Th via neutron irradiation of a ^{226}Ra target in a nuclear reactor, through the ^{226}Ra(3n,2β)^{229}Th reaction, yields about 1,000-fold greater activity levels of ^{228}Th ($t_{1/2}$ = 1.9125 ± 0.0009 y) than ^{229}Th, and the 2.6 MeV γ-ray in the ^{228}Th decay chain [this γ-ray actually originates from the decay of ^{208}Tl, ($t_{1/2}$ = 3.053 ± 0.004 min) following de-excitation of the 1st excited state (2614.551 keV, 16.7 ps, 3$^-$) of ^{208}Pb] poses shielding problems for large-scale production via this route [22,24,29].

Although the yield of ^{225}Ra and ^{225}Ac produced from the direct production is significantly higher than the indirect route (i.e., decay of ^{229}Th), the required fast turnaround for processing the radium target in the direct production of ^{225}Ra and ^{225}Ac (a few days post-irradiation) is the main disadvantage for proton and γ-ray irradiation of a ^{226}Ra target, and proton spallation of ^{232}Th target [15]. Continuous processing of radium targets for the direct production of ^{225}Ra and ^{225}Ac is far more challenging than routine extraction of ^{225}Ra and ^{225}Ac from the long-lived ^{229}Th. Further, simultaneous production of large quantities of fission products in the high-energy (E_p > 100 MeV) proton-irradiated ^{232}Th target is an additional complexity associated with this approach. Developing a stockpile of ^{229}Th may prove to be the best means of providing ^{225}Ra and ^{225}Ac in the long term.

As an alternative to the production methods currently being pursued, ^{229}Th can be produced by proton bombardment of ^{230}Th and ^{232}Th targets. Among possible reactions, (p,2n) and (p,4n) reactions on ^{230}Th and ^{232}Th targets, respectively, are of main interest in proton energies below 50 MeV. These reactions can yield ^{229}Pa, which decays via electron capture (EC, 99.5%) to ^{229}Th with a half-life of 1.5 d. Protactinium-229 also decays via α-emission to ^{225}Ac with a branching ratio previously measured at 0.5% [30]. At somewhat higher energies, the contribution of ^{232}Th(p,α)^{229}Ac($t_{1/2}$ = 62.7 ± 0.5 min, β^-)^{229}Th, ^{232}Th(p,p3n)^{229}Th, and ^{230}Th(p,2p)^{229}Ac reactions to the overall yield of ^{229}Th cannot be ignored. A summary of the threshold energies and coulomb barriers for possible reactions leading to the formation of ^{229}Th in proton bombardment ($E_p \leq 40$ MeV) of ^{232}Th targets are given in Table I. Fig. S1 of the Supplemental Material [31] is a graphic representation of the chart of the nuclides that facilitates interpretation of the various

reactions leading to the formation of ^{229}Th from ^{230}Th and ^{232}Th. Although $^{228\ \&\ 230}$Pa can be readily quantified by their corresponding γ rays in the chemically purified Pa, ^{229}Pa is barely detectable in the presence of other protactinium isotopes because of its exceedingly weak γ rays. In fact, the reported γ rays following the decay of ^{229}Pa were obtained from highly pure mass-separated sources of ^{229}Pa [30], but no excitation functions for these reactions have been reported.

We report the excitation functions for proton-induced reactions on natural thorium yielding to $^{228,\ 229,\ 230\ \&\ 232}$Pa isotopes; ^{232}Th(p,xn) reactions, where x = 1, 3, 4, and 5, at proton energy ranges of 12–40 MeV. We also report the effective production cross section for the ^{232}Th(p,x)^{229}Th reaction from 23–33 MeV. With the exception to the ^{232}Th(p,3n)^{230}Pa reaction, excitation functions for other ^{232}Th(p,xn) reactions are reported for the first time. These experimental data are compared with theoretical cross section calculations using the simulation codes PHITS and MCNP6. The half-life and α-branching ratio, α/(α + EC) of ^{229}Pa were also evaluated.

II. EXPERIMENTAL PROCEDURES

A. Materials and equipment

Natural thorium foils, (99.9%, ~0.0125 and 0.125 mm thick) were obtained from Goodfellow Cambridge Ltd. (Ermine Business Park, Huntingdon, England PE29 6WR). High-purity (99.95%) aluminum foils used as energy degraders were obtained from Alfa Aesar (26 Parkridge Road, Ward Hill, MA 01835).

The ion exchange resins MP1 (Cl^- form, 200–400 mesh) and AG50X4 (H^+ form, 200–400 mesh), and disposable polypropylene columns (2 mL bed volume [BV] and a 0.8 cm inner diameter) were purchased from Bio-Rad Laboratories (4000 Alfred Nobel Drive, Hercules, CA 94547), and resins were stored in deionized water. As needed the MP1 resin in chloride form was converted to nitrate form by washing the resin with 4 BV of 8 *M* HNO_3, followed by 4 BV of deionized water and the nitrate converted resin was always stored in deionized water. The column used for chemical processing of the thin target was a 0.4 mL MP1/Cl^- column, pre-equilibrated with 1 mL of 10 *M* HCl before use. In processing of the thick target, three separate columns were used: Column A was a 0.4 mL MP1/Cl^- as above, column B was a 3 mL BV

MP1/NO_3 pre-equilibrated with 8 *M* HNO_3 before use, and column C was the same as column B except 0.5 mL BV.

B. Targets

Targets consisted of four assemblies of stacked foils. The first two assemblies were considered the "thin targets" (0.0125 mm thick). The first assembly consisted of eight natural thorium foils (18.5–21.6 mg cm^{-2}), and the second assembly consisted of five foils. Each of the thorium foils was mounted on a thin (0.025 mm) high-purity aluminum foil disk. The thorium foils were 1.25 × 1.25 cm squares, whereas the aluminum foil disks had a diameter of 4 cm. Varying thicknesses of 4 cm diameter high-purity aluminum foil disks were placed between the thorium foils to optimize the proton energy loss throughout the target stack. Each target stack was enclosed in a circular aluminum target holder with a 2-cm diameter hole at the center allowing for beam access. Typical beam diameters for the tandem accelerator are on the order of 8 mm. The target holder is shown in Fig. S2 of the Supplemental Material, and the full assembly at the Holifield Radioactive Ion Beam Facility is shown in Fig. S3 of the Supplemental Material [31].

The third and fourth sets of assemblies, considered the "thick targets" (0.125 mm thick), were constructed using the stacked foil technique as well, but without any aluminum degraders. For the third assembly, twenty-three 1 × 1 cm square thorium foils (137 mg cm^{-2} each) were stacked for a total thickness (areal density) of 3.15 g cm^{-2}. The fourth and final assembly was identical to the third assembly except with 4 foils instead of 23 (areal density = 0.55 g cm^{-2}). A circular aluminum target holder with the exact same dimensions as used in the thin target experiments was used in the thick target experiments. The mass and areal density of each of the foils was determined with less than 1% uncertainty. Degradation of proton energies in each target stack was calculated using the Stopping and Range of Ions in Matter (SRIM) code [32]. Details on the associated uncertainty of these calculated proton energies can be found in Ref [33].

C. Radioactivity measurements

The activity measurements for both the thin target and thick target experiments were performed with a calibrated high-purity intrinsic germanium detector coupled to a PC-based multichannel analyzer using Genie 2000 software (Canberra Industries, 800 Research Parkway, Meriden, CT

06450). The resolution of the detector is 0.74 keV at 122 keV and 2.0 keV at 1332 keV. The detector energy and efficiency calibrations were performed using γ-ray sources traceable to the National Institute of Standards and Technology.

The specific γ rays and their corresponding intensities used to assay the radioisotopes involved in this work are shown in the Table S1 of the Supplemental Material [31]. These data were taken from the Nuclear Data Sheets [34-38]. For the thin targets, the activity of ^{229}Pa was measured using the 117.2 and 119.0 keV γ rays post chemical separation of the protactinium from fission products and other actinides (see chemical separation section). The efficiency of chemical separation (chemical yield) was calculated using the 952 keV (29.6%) γ ray from ^{230}Pa ($t_{1/2}$ = 17.4 ± 0.5 d) before and after chemical separation. When possible, all activities were measured over several half-lives and the activities at the end of bombardment (A_0) were extrapolated by a modified Brookhaven Decay Curve Analysis Program (CLSQ) [39]. Radioactivity (counts per second) at the end of bombardment was converted to absolute disintegrations per second (A_0) by appropriate corrections for the γ-ray intensity and detector efficiency. When necessary, appropriate corrections were applied for radioactivity decay during counting time using the following equation

$$A_0 = \frac{\lambda_i C}{\left(1 - e^{-\lambda_i t}\right) \varepsilon P_\gamma} \ , \qquad (1)$$

where A is radioactivity, C is the uncorrected count rate, t is the count time, ε is the energy-dependent detector efficiency, and P_γ is the absolute γ ray emission probability. For the thick target experiments the activity of ^{229}Th was determined using the 193.59 keV (4.41%) γ ray. Because the activity of ^{229}Th produced in the target was 2–3 orders of magnitude lower than activity of other isotopes (reflecting the long half-life of ^{229}Th), chemical separation of thorium from fission products and ^{228}Th decay daughters was also necessary. In this case, the chemical yield was determined by using the 238.58 keV (43.6%) γ ray from the decay of ^{212}Pb ($t_{1/2}$ = 10.64 ± 0.01 h, the 238.58 keV γ ray originates from excited state of ^{212}Bi following β^- decay of ^{212}Pb in the decay chain of ^{228}Th). The 3-month delay between the end of bombardment and chemical processing ensured that ^{212}Pb was in secular equilibrium with its parent radioisotope, ^{228}Th.

D. Irradiations

The irradiations were conducted at the On-Line Test Facility, a low-intensity Isotope Separation On-Line facility primarily used for testing of ion sources and targets for the production of radioactive ion beams located at Oak Ridge National Laboratory's recently decommissioned Holifield Radioactive Ion Beam Facility [40]. Proton beams of up to 40 MeV in energy and 50 nA of intensity were delivered from the tandem accelerator [41].

For the cross section measurements, the targets were stacked in an aluminum holder that was mounted in a copper fixture in the facility's standard target-ion source enclosure (see Figs. S2 and S3 of the Supplemental Material [31]). A Faraday cup was positioned directly behind the target for continuous monitoring of the proton beam during irradiation. The copper mounting fixture was connected to a water-cooled copper feed-through to provide target cooling. However, water cooling was not required for the targets. The tandem beamline connecting to the enclosure contains diagnostics to measure the size, position, and intensity of the beam just before entering the target. The proton beam scatters in the thick target, so only a fraction of the beam is observed in the Faraday cup after the target. This fraction depends on beam energy and thickness of the target. Periodic measurements of the beam currents before and after the target allow for a determination of the fraction of beam observed in the Faraday cup after the target. This ratio coupled with the continuous measurement of the current after the target provides for a precise calculation of the number of protons hitting the target.

Irradiation periods ranged from several hours to a few days, depending on the half-lives of the nuclei of interest. After the end of irradiation, the stack of targets was removed from the aluminum holder, and individual target foils were mounted on counting cards for measurements.

For each irradiation, 40 MeV proton beams were used that had an average current of 45–50 nA. The total accumulated charge for the thin target experiments was 2.56 μA/h, and the total accumulated charge for the thick target experiments was 8.69 μA/h. To validate our technique for measuring cross section data (with regard to proton energy and beam intensity), copper and nickel targets were irradiated under identical conditions, and the excitation functions of a number

of reactions were determined and found to be in excellent agreement (within acceptable uncertainty) with those reported in the literature. The corresponding data is presented in [33].

E. Chemical separations

Although $^{228\ \&\ 230}$Pa can be directly quantified in the irradiated thorium target, ^{229}Pa emits only exceedingly weak γ rays and is undetectable in the presence of other protactinium isotopes and the fission products. Therefore, chemical separation is necessary to observe ^{229}Pa. Post-irradiation, the thin targets underwent one round of data collection; γ-ray spectra of individual target foils were taken for ~30 min each. Then, approximately 24 hours after the end of bombardment, the targets were dissolved, and the protactinium fraction was purified using column chromatography, precipitated with $Fe(OH)_3$, and mounted for γ-ray analysis. Protactinium-230 activity in the thorium foils before and after chemical processing was used to obtain the overall chemical yields, which ranged from 65%–80%. After two further rounds of data collection and about a week of decay, ^{225}Ac (the α-decay product of ^{229}Pa, 0.5%) was extracted from ^{229}Pa samples by redissolving the precipitated protactinium samples and separating ^{225}Ac by column chromatography. The protactinium fraction was also reprecipitated and mounted for counting. This process was later repeated using a pure sample of ^{225}Ac to determine the overall chemical yield.

Because of high background radiation and low activity, direct measurement of ^{229}Th (the EC decay daughter of ^{229}Pa) is not possible for the thick targets, and ^{229}Th was only observable by a two-stage chemical purification of the target material. High background primarily originates from ^{228}Th decay daughters (^{224}Ra, ^{212}Pb, ^{212}Bi, and ^{208}Tl) and long-lived fission products. Further, the time window for observing ^{229}Th is limited to about 12 h after chemical separation because the ^{228}Th decay daughters will grow back very quickly. The chemical processing of the thick target was more extensive than the thin target and was based on a series of ion exchange chromatography separations. A γ-ray spectrum of the highly purified thorium sample was taken immediately, and the sample in liquid form (1.5 mL) in a 20 mL Pyrex scintillation vial was analyzed at 2 cm from the surface of the detector for 5 h. Although multiple 5-h spectra were taken, the 193.52 keV γ ray for ^{229}Th only was observable in the first few spectra primarily because of the ingrowth of ^{212}Pb and ^{212}Bi, the decay daughters of ^{228}Th. The 210.85 keV γ ray

emitted by ^{229}Th was not used for this assay because ^{227}Th ($t_{1/2}$ = 18.697 ± 0.007 d), produced directly via ^{232}Th(p,p5n) or indirectly from β^--decay of ^{227}Ac ($t_{1/2}$ = 21.772 ± 0.003 y), produced via ^{232}Th(p,α2n) also emits a 210.62 keV γ ray (1.25%). A brief description of the chemical processing of the target is given in the Supplemental Material [31], and the full details can be found in Ref. [42].

III. RESULTS

A. Cross sections of protactinium isotopes from ^{232}Th

The measured cross sections for proton-induced reactions on natural thorium yielding to ^{228,229,230,232}Pa isotopes (^{232}Th(p,xn)Pa reactions, where x = 1, 3, 4, and 5) are given in Table II. These data were obtained in four sets of independent experiments in which proton energy ranged from 12–40 MeV. As indicated in the first column of Table II, the proton energy loss in each foil was ~2 MeV per foil at incident proton energy of 40 MeV, which increases to ~4 MeV per foil at 13 MeV where the protons exited the stacked foil target. The corresponding excitation functions are shown in Figs. 1–4. With the exception to the ^{232}Th(p,3n)^{230}Pa reaction [43], the excitation functions for the other ^{232}Th(p,x) reactions are reported for the first time for this proton energy range. The data for the ^{232}Th(p,n)^{232}Pa, ^{232}Th(p,3n)^{230}Pa, and ^{232}Th(p,5n)^{228}Pa reactions were deduced by direct analysis of the thorium foils after irradiation, and the excitation functions for these reactions, measured in three independent experiments, were within the statistical errors. All cross section uncertainties are quoted with sigma = 1. As shown in Fig. 1, the excitation function of the ^{232}Th(p,5n)^{228}Pa reaction peaks at 78.9 ± 0.4 mb and E_p = 38.0 ± 0.3 MeV. For the ^{232}Th(p,3n)^{230}Pa reaction, the peak of 372 ± 20 mb occurs at E_p = 21.2 ± 0.5 MeV. Our data for this reaction are in excellent agreement with the reported excitation function in the 17–40 MeV proton energy range, with one additional point at 13 MeV (Figs. 1 and 3) [43]. For the ^{232}Th(p,n)^{232}Pa reaction, in the 12–40 MeV energy range, the excitation function remains flat at 10–17 mb.

The excitation function for the ^{232}Th(p,4n)^{229}Pa reaction (Figs. 1–2) was obtained by chemically extracting protactinium from the thorium target foils. The peak of excitation function for this reaction occurs at 162 ± 14 mb and E_p = 29.7 ± 0.5 MeV. As noted earlier, the ^{230}Pa activities in

the thorium foils before and after chemical processing were used to obtain the overall chemical yields, which ranged from 65%–80%.

B. Half-life and α-branching ratio of ^{229}Pa

The half-life of ^{229}Pa was remeasured in four purified samples of protactinium fraction by following the decay of the 117.2 and 119.0 keV γ rays for approximately four half-lives. A CLSQ [39] input file was created for each photopeak from each sample for a total of eight input files. This generated a total of eight half-life data points and associated uncertainties. A weighted average of the half-life μ' was calculated using the inverse of the square of the individual errors as the weighing factor:

$$\mu' = \frac{\sum\left(x_i / \sigma_i^2\right)}{\sum\left(1/\sigma_i^2\right)}, \tag{2}$$

where x_i and σ_i are the independently calculated half-life and the associated uncertainty, respectively. A summary of the results for the samples is given in Table III, and the data is plotted in Fig. 5. The least square fit weighted average of all the data points (solid line) produced a value of 1.55 ± 0.01 d.

As pointed out earlier, after about a week of decay, the purified ^{229}Pa sample was dissolved, and ^{225}Ac was extracted from ^{229}Pa samples. A typical spectrum of ^{225}Ac showing two predominate γ rays at 218.0 and 440.45 keV (from 4.8-min ^{221}Fr and 45-min ^{213}Bi) is depicted in Fig. 6. The chemical yield for this process was 92 ± 4%, and it was estimated from three mock reactions tagged with microcurie amounts of ^{225}Ac, which is routinely available from Oak Ridge National Laboratory (https://www.isotopes.gov/ibo/ibo.html). The α-branching ratio, α/(α + EC), of ^{229}Pa was measured by radiochemical techniques and found to be 0.53 ± 0.10%.

C. Effective cross section of ^{229}Th from thick ^{232}Th target

The excitation function for the thick target ^{232}Th(p,x)^{229}Th reaction is shown in Fig. 8. Effective cross sections from the thick target experiment are slightly higher than the values obtained for the ^{232}Th(p,4n)^{229}Pa reaction. However, this is to be expected because of the effective cross

section containing all possible production pathways for the ^{232}Th(p,x)^{229}Th reaction. A weighted average approach was used to combine the results of two separate irradiations at four incident proton energies (25.8–29.6 MeV, Table IV).

One of the largest difficulties in determining the effective cross section for the ^{232}Th(p,x)^{229}Th reaction is the ability to measure the 193.52 keV γ ray emitted by ^{229}Th. The spectra of the thorium foil from the thick target experiment at 6 months post EOB and before ^{212}Pb removal is shown in Fig. 7a. Fig. 7b shows a spectrum of the purified thorium fraction after removal of >99% of ^{212}Pb by chemical processing. As shown in Fig. 7a, the 193.52 keV γ ray from the decay of ^{229}Th is not visible due to the Compton continuum generated by γ-ray emissions from ^{228}Th decay daughters. In Fig. 7b the 193.52 keV γ ray from the decay of ^{229}Th is clearly visible but only for a short time until ^{228}Th decay daughters grow into equilibrium with ^{228}Th. In this case, each sample was assayed directly after (usually less than 1 day) chemical separation to allow for as much measurement time as possible before ^{212}Pb grew back into secular equilibrium with ^{228}Th. Despite this, only a low count rate ($<5 \times 10^{-3}$ counts per second in some cases) was observed for the 193.52 keV γ-ray peak of each sample. For this reason, ^{229}Th was only verified to be present in measurable quantities in 9 of the 23 foils. The low number of counts also contributed to the large uncertainty shown in Fig. 8 for the ^{232}Th(p,x)^{229}Th reaction cross sections.

D. Theoretical cross section calculations with PHITS and MCNP6

The theoretical prediction of the production cross sections for protactinium isotopes was calculated by the Monte Carlo–based particle transport simulation codes PHITS [44] and MCNP6 [45]. PHITS is a Monte Carlo–based particle transport simulation code managed by the Japan Atomic Energy Agency that can process the transport of particles as well as the collisions of particles with target nuclei. PHITS is capable of calculating the transport of nuclei, nucleons, photons, electrons, and mesons. The continuous-slowing approximation is applied to charged particle transport using the computer code Stopping Powers and Ranges (SPAR) [46]. For these calculations, PHITS Version 2.64 was employed through a combination of the intra-nuclear cascade (INCL 4.6) and evaporation (GEM) models to determine the proton reaction cross

sections of the irradiations occurring in the 10–40 MeV incident proton energy range [47]. It is important to note that the PHITS output includes only radionuclides produced independent of decay, whereas the thick target experimental effective cross sections for the ^{232}Th(p,x)^{229}Th reaction reported in this work are considered cumulative.

For charged particle energies below the 1 GeV range, MCNP6 employs the Cascade-Exciton Model (CEM), specifically CEM 3.03 [48]. Through this event-generator, MCNP6 simulates nuclear reactions in a three-stage process. Like PHITS, the first stage involves the intra-nuclear cascade model where the primary particle (i.e., incident proton) scatters multiple times within the nucleus and produces secondary particles several times before being absorbed by the nucleus or escaping it entirely. The second stage employs the coalescence model to generate high-energy particles up to $A \leq 4$. Simultaneously, these high-energy particles escape and leave the residual nucleus in the pre-equilibrium stage that is simulated by the modified exciton model. Equilibrium evaporation or fission comprises the final stage of the CEM3.03 model. As with PHITS, the residual nuclei tallied in the MCNP6 output includes radionuclides generated independent of radioactive decay.

IV. DISCUSSION

In this study, we have reported excitation functions for ^{228}Pa, ^{229}Pa, ^{230}Pa, and ^{232}Pa produced via proton-induced reactions on natural thorium, specifically ^{232}Th(p,xn) reactions, where x = 1, 3, 4, and 5, at proton energy ranges of 12–40 MeV. We have also measured the effective production cross section of ^{229}Th from the irradiation of thick ^{232}Th targets. The effective cross section includes contribution from the ^{232}Th(p,4n)^{229}Pa ($t_{1/2}$ = 1.5 d, EC)^{229}Th, ^{232}Th(p,p3n)^{229}Th, and ^{232}Th(p,α)^{229}Ac($t_{1/2}$ = 62.7 m, β^-)^{229}Th reactions. The measurement of the total ^{229}Th production yield also allows for a good estimate of the feasibility of production in an accelerator unlike other methods currently being investigated.

As detailed in the preceding sections, sources of ^{229}Pa were produced by the ^{232}Th(p,4n)^{229}Pa reaction after a two-step chemical purification, and the half-life and α-branching ratio, α/(α + EC), of ^{229}Pa were measured to be 1.55 ± 0.01 d and 0.53 ± 0.10%, respectively. Our measured half-life and α-branching ratio are in relative agreement with the reported value of 1.50

± 0.05 d and 0.48 ± 0.05% (obtained from γ-α coincidence measurement) of a mass separated sample of ^{229}Pa [30]. The excitation function for this reaction, determined from the thin target measurement, reaches a peak of 162 ± 14 mb at E_p = 29.7 ± 0.5 MeV. The slightly higher thick target cross sections for this reaction (Figs. 2 and 8) again indicates the ^{232}Th(p,4n)^{229}Pa reaction is the major reaction pathway for the cumulative ^{232}Th(p,x)^{229}Th reaction cross section. This is likely because of the high exit coulomb barrier energy for the ^{232}Th(p,α)^{229}Ac(62.7 m, β^-)^{229}Th and ^{232}Th(p,p3n)^{229}Th reactions (Table I). Similarly, Table I shows that there are many exit channels leading to the formation of ^{229}Th. Although the threshold energy for many of these reactions is low, the coulomb barrier of particles exiting the nucleus are much higher.

Each of the theoretical cross sections reported in Figs. 1–4 and Fig. 8 are directly produced independent cross sections with the exception of the ^{232}Th(p,x)^{229}Th cumulative cross section. This cumulative cross section is a summation of the ^{232}Th(p,4n)^{229}Pa, ^{232}Th(p,p3n)^{229}Th, and the ^{232}Th(p,α)^{229}Ac reaction cross sections. The PHITS predicted cross sections agree with the experimental measurements and support the fact that the ^{232}Th(p,4n)^{229}Pa reaction is the predominant pathway for the cumulative ^{232}Th(p,x)^{229}Th reaction below 30 MeV. Above 33 MeV, PHITS predicts a rise in cross sections for the ^{232}Th(p,p3n)^{229}Th reaction. This increase in cross section is predicted from systematics based on similar reactions of slightly lower mass targets [49,50]. However, we were not able to experimentally measure this rise because of the significant increase in ^{228}Th activity (produced mostly via the ^{232}Th(p,5n)^{228}Pa ($t_{1/2}$ = 22 ± 1 h, EC)^{228}Th reaction), masking the detection of both ^{229}Pa and ^{229}Th radionuclides by γ-ray spectroscopy in the thick target experiment. Note that although experimental data is lacking in proton energy above 30 MeV, the theoretical cross sections for the ^{232}Th(p,x)^{229}Th, ^{232}Th(p,4n)^{229}Pa, ^{232}Th(p,α)^{229}Ac, and ^{232}Th(p,p3n)^{229}Th reactions are shown in Fig. 8 and Fig. S4 of the Supplemental Material [31]. The independent cross sections generated by MNCP6 for the ^{232}Th(p,4n)^{229}Pa reaction are a factor of two higher than the experimentally measured, and PHITS generated cross sections for this reaction from 20 to 35 MeV. Similarly, the peak of the theoretical excitation function generated by MCNP6 for the ^{232}Th(p,3n)^{230}Pa reaction is about 60% higher than the same excitation function generated by PHITS (Fig. 3). However, at incident proton energies >30 MeV MCNP6 fits more closely with the experimental data for the ^{232}Th(p,3n)^{230}Pa reaction. In general, there is little agreement between PHITS and MCNP6 for all

of the ^{232}Th(p,xn)Pa reactions over the observed energy range. One possible explanation for this discrepancy is the use of different physics models in their event generators.

Based on the ^{232}Th(p,x)^{229}Th reaction excitation function experimentally measured and shown in Fig. 8, a 1-year irradiation of a thick thorium foil target (2.34 g cm^{-2}) with an incident proton beam of 40 MeV and 200 μA would yield ~31 mCi of ^{229}Th, which is enough ^{229}Th to produce ~10 mCi of ^{225}Ac every 20 days.

ACKNOWLEDGMENTS

This research was supported by the Office of Nuclear Physics of the US Department of Energy. The authors acknowledge the efforts of the Holifield Radioactive Ion Beam Facility staff in delivering the high-quality proton beams that made this study possible.

REFERENCES

[1] G. Sgouros, Adv. Drug Delivery Rev. **60**, 1402 (2008).
[2] D. A. Mulford, D. A. Scheinberg, and J. G. Jurcic, J. Nucl. Med. **46**, 199S (2005).
[3] B. J. Allen, Z. Tian, S. M. A. Rizvi, Y. Li, and M. Ranson, Br. J. Cancer **88**, 944 (2003).
[4] S. J. DeNardo, Semin. Nucl. Med. **35**, 143 (2005).
[5] L. E. Feinendegen and J. J. McClure, Radiation Research Society, Denver, CO, 195-201 (1997).
[6] C. Kratochwil *et al.*, J. Nucl. Med. **57**, 1941 (2016).
[7] B. M. Sandmaier, W. A. Bethge, D. S. Wilbur, D. K. Hamlin, E. B. Santos, M. W. Brechbiel, D. R. Fisher, and R. Storb, Blood **100**, 318 (2002).
[8] T. K. Stutchbury, F. Al-ejeh, G. E. Stillfried, D. R. Croucher, J. Andrews, D. Irving, M. Links, and M. Ranson, Mol. Cancer Ther. **6**, 203 (2007).
[9] S. J. Kennel, R. Boll, M. Stabin, H. M. Schuller, and S. Mirzadeh, Br. J. Cancer **80**, 175 (1999).
[10] E. Dadachova *et al.*, PLOS Med. **3**, e427 (2006).
[11] D. E. Bergeron and R. Fitzgerald, Appl. Radiat. Isot. **102**, 74 (2015).
[12] S. M. Collins, A. K. Pearce, K. M. Ferreira, A. J. Fenwick, P. H. Regan, and J. D. Keightley, Appl. Radiat. Isot. **99**, 46 (2015).
[13] S. M. Collins, A. K. Pearce, P. H. Regan, and J. D. Keightley, Appl. Radiat. Isot. **102**, 15 (2015).
[14] O. Couturier, S. Supiot, M. Degraef-Mougin, A. Faivre-Chauvet, T. Carlier, J. F. Chatal, F. Davodeau, and M. Cherel, Eur. J. Nucl. Med. Mol. Imaging **32**, 601 (2005).
[15] S. Mirzadeh, Appl. Radiat. Isot. **49**, 345 (1998).
[16] M. Miederer, D. A. Scheinberg, and M. R. McDevitt, Adv. Drug Delivery Rev. **60**, 1371 (2008).
[17] M. R. McDevitt, D. Ma, J. Simon, R. K. Frank, and D. A. Scheinberg, Appl. Radiat. Isot. **57**, 841 (2002).
[18] M. Cherel, F. Davodeau, F. Kraeber-Bodere, and J. Chatal, J. Nucl. Med. Mol. Imaging **50**, 322 (2006).
[19] M. W. Brechbiel, Dalton Transactions, 4918 (2007).
[20] H. Kikunaga, T. Suzuki, M. Nomura, T. Mitsugashira, and A. Shinohara, Phys. Rev. C **84**, 014316 (2011).
[21] R. A. Boll, D. Malkemus, and S. Mirzadeh, Appl. Radiat. Isot. **62**, 667 (2005).
[22] R. A. Boll, M. A. Garland, and S. Mirzadeh, in *ANS Annual Meeting: Isotopes for Medicine and Industry* ANS, Anaheim, CA, (2008).
[23] IAEA, Technical Meeting on Alpha Emitting Radionuclides and Radiopharmaceuticals, Vienna, (2013).
[24] S. Hogle, R. A. Boll, K. Murphy, D. Denton, A. Owens, T. J. Haverlock, M. Garland, and S. Mirzadeh, Appl. Radiat. Isot. **114**, 19 (2016).
[25] J. R. Griswold *et al.*, Appl. Radiat. Isot. **118**, 366 (2016).
[26] J. W. Weidner *et al.*, Appl. Radiat. Isot. **70**, 2590 (2012).
[27] J. W. Weidner *et al.*, Appl. Radiat. Isot. **70**, 2602 (2012).
[28] S. V. Ermolaev, B. L. Zhuikov, V. M. Kokhanyuk, V. L. Matushko, N. Kalmykov Stepan, A. Aliev Ramiz, G. Tananaev Ivan, and F. Myasoedov Boris, Radiochim. Acta **100**, 223 (2012).
[29] M. J. Martin, Nucl. Data Sheets **108**, 1583 (2007).

[30] I. Ahmad, J. E. Gindler, A. M. Friedman, R. R. Chasman, and T. Ishii, Nucl. Phys. A **472**, 285 (1987).
[31] See Supplemental Material at [URL will be inserted by publisher] for additional experimental information including details about the chemical separation of protactinium from throium.
[32] J. F. Ziegler, J. P. Biersack, and U. Littmark, *The Stopping and Range of Ions in Solids* Pergamon Press, New York, (1985).
[33] C. U. Jost, J. R. Griswold, S. H. Bruffey, S. Mirzadeh, D. W. Stracener, and C. L. Williams, AIP Conference Proceedings: International Conference on Application of Accelerators in Research and Industry, **1525**, 520 (2013).
[34] E. Browne, Nucl. Data Sheets **104**, 427 (2005).
[35] A. Artna-Cohen, Nucl. Data Sheets **80**, 723 (1997).
[36] E. Browne and J. K. Tuli, Nucl. Data Sheets **109**, 2657 (2008).
[37] E. Browne and J. K. Tuli, Nucl. Data Sheets **113**, 2113 (2012).
[38] E. Browne, Nucl. Data Sheets **107**, 2579 (2006).
[39] J. B. Cumming, in *Applications of Computers to Nuclear and Radiochemistry*, edited by G. D. O'Kelley (1962).
[40] H. K. Carter and D. W. Stracener, Nucl. Instrum. Methods B **266**, 4702 (2008).
[41] M. J. Meigs, D. L. Haynes, C. M. Jones, and R. C. Juras, Nucl. Instrum. Methods A **382**, 51 (1996).
[42] J. R. Griswold, M. S. thesis, University of Tennessee, 2014.
[43] A. Morgenstern, C. Apostolidis, F. Bruchertseifer, R. Capote, T. Gouder, F. Simonelli, M. Sin, and K. Abbas, Appl. Radiat. Isot. **66**, 1275 (2008).
[44] T. Sato *et al.*, J. Nucl. Sci. Technol. **50**, 913 (2013).
[45] T. Goorley *et al.*, Nucl. Technol. **180**, 298 (2012).
[46] T. W. Armstrong, K. C. Chandler, Oak Ridge National Laboratory ORNL-4869, (1973).
[47] A. Boudard, J. Cugnon, J. C. David, S. Leray, and D. Mancusi, Phys. Rev. C **87**, 014606 (2013).
[48] S. G. Mashnik, K. K. Gudima, R. E. Prael, A. J. Sierk, M. I. Baznat, and N. V. Mokhov, in *Joint ICTP-IAEA Advanced Workshop on Model Codes for Spallation Reactions* Trieste, Italy, (2008).
[49] C. Birattari, M. Bonardi, and M. C. Gilardi, Radiochem. Radioanal. Lett. **49**, 25 (1981).
[50] M. C. Lagunas-Solar, O. F. Carvacho, L. Nagahara, A. Mishra, and N. J. Parks, Int. J. Radiat. Applic. Instrum. A **38**, 129 (1987).
[51] Q-value Calculator (QCalc), http://www.nndc.bnl.gov/qcalc/.

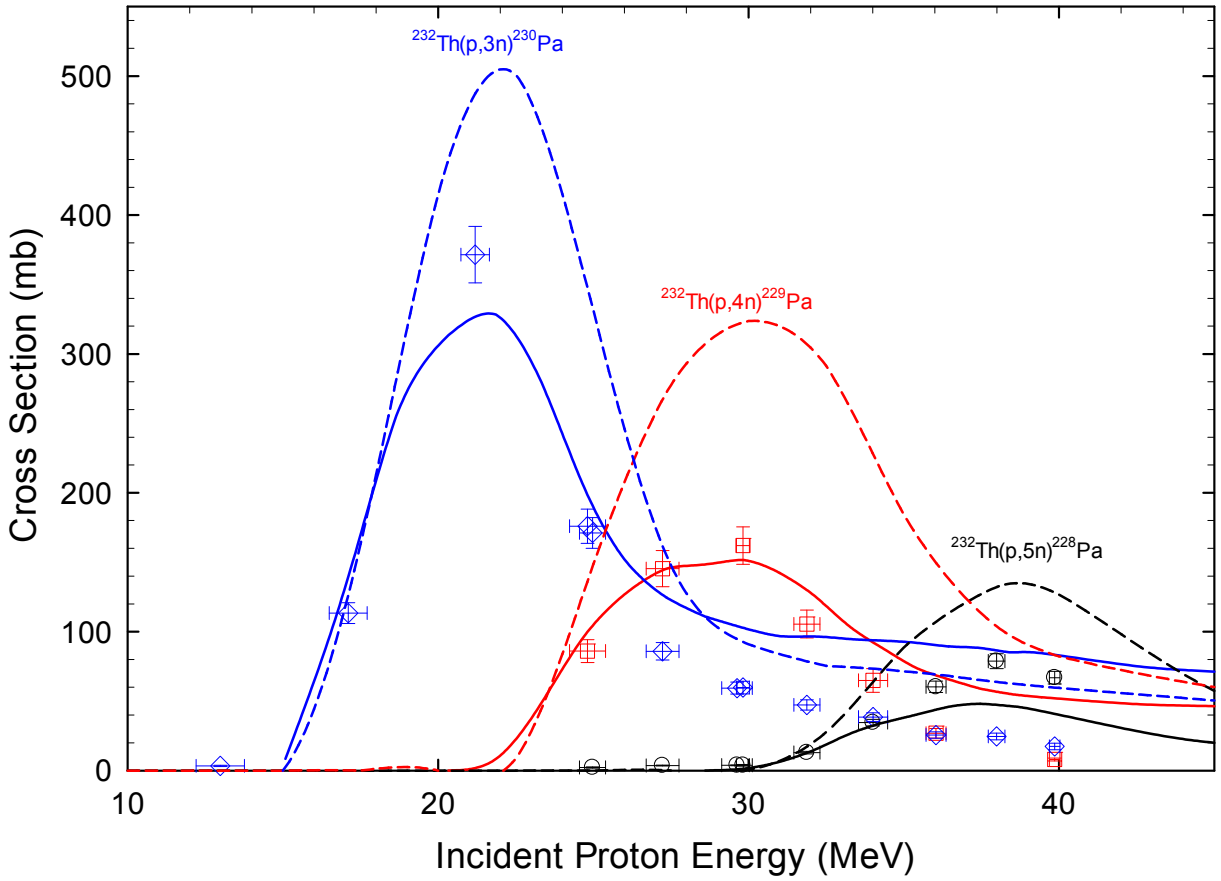

FIG. 1. A comparison of the experimental excitation functions for the ^{232}Th(p,3n)^{230}Pa reaction (blue diamonds), the ^{232}Th(p,4n)^{229}Pa reaction (red squares), and the ^{232}Th(p,5n)^{228}Pa reaction (black circles) with the theoretical PHITS (solid curves) and MCNP6 (dashed curves) excitation functions.

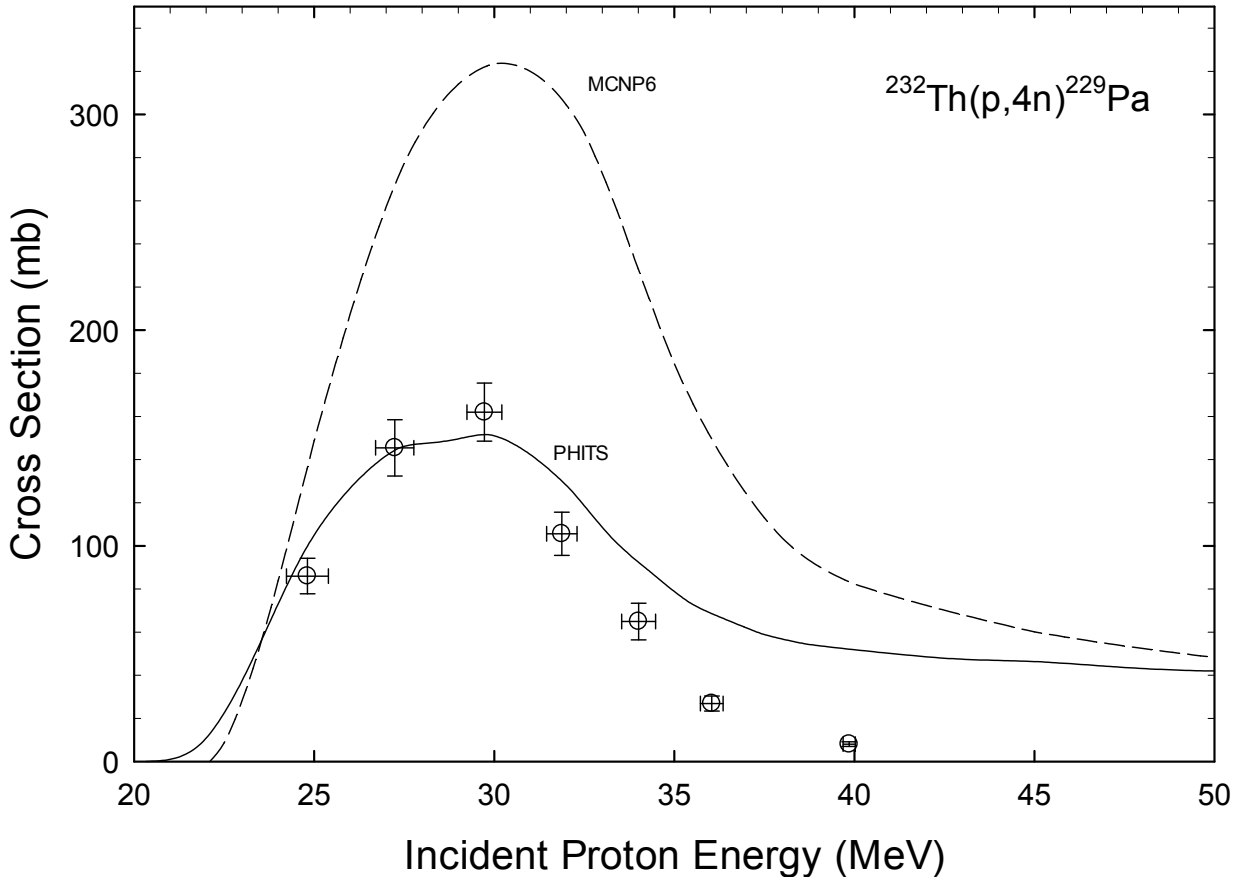

FIG. 2. A comparison of the experimental (data points) and theoretical PHITS (solid curves) and MCNP6 (dashed curves) excitation functions for the ^{232}Th(p,4n)^{229}Pa reaction.

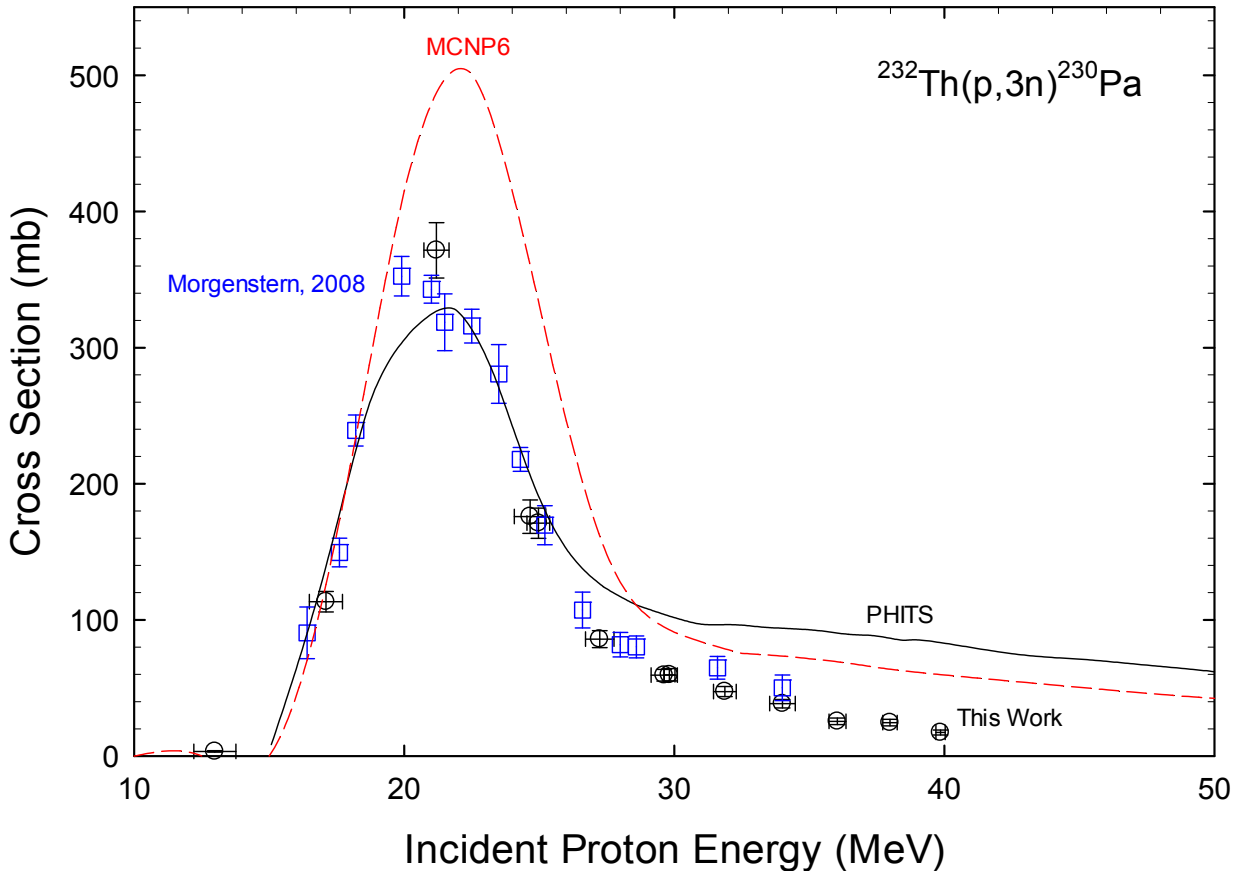

FIG. 3. A comparison of the experimental (black circles) and theoretical PHITS (solid curves) and MCNP6 (dashed curves) excitation functions for the ^{232}Th(p,3n)^{230}Pa reaction. Also included is the previous measurement in Ref. [43] (blue squares).

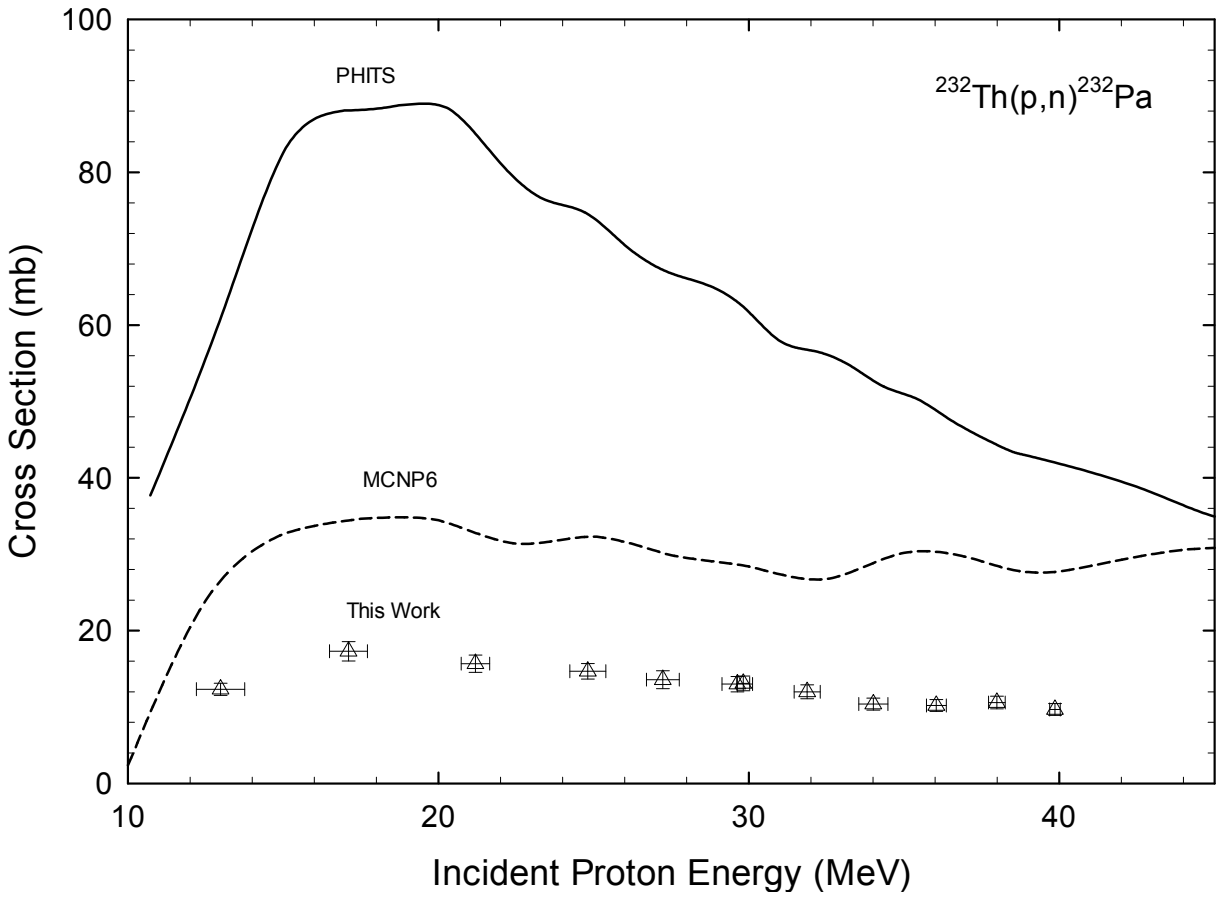

FIG. 4. A comparison of the experimental (data points) and theoretical PHITS (solid line) and MCNP6 (dashed line) excitation functions for the ^{232}Th(p,n)^{232}Pa reaction.

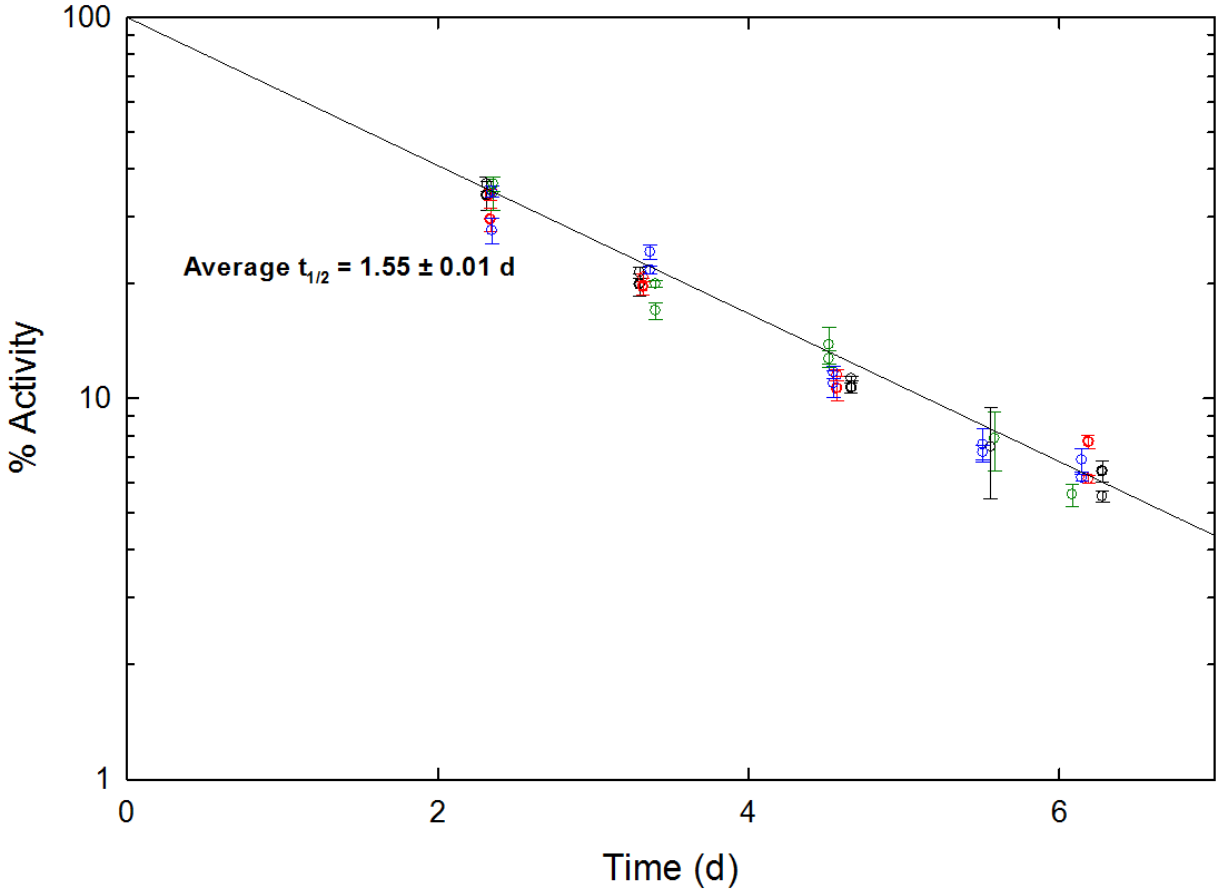

FIG. 5. Half-life of ^{229}Pa using the 117.2 keV (0.05%) and 119.0 keV (0.13%) γ rays. CLSQ code was used for a least square fit of the decay of the two γ rays. Each color represents an independent sample used to calculate the weighted average.

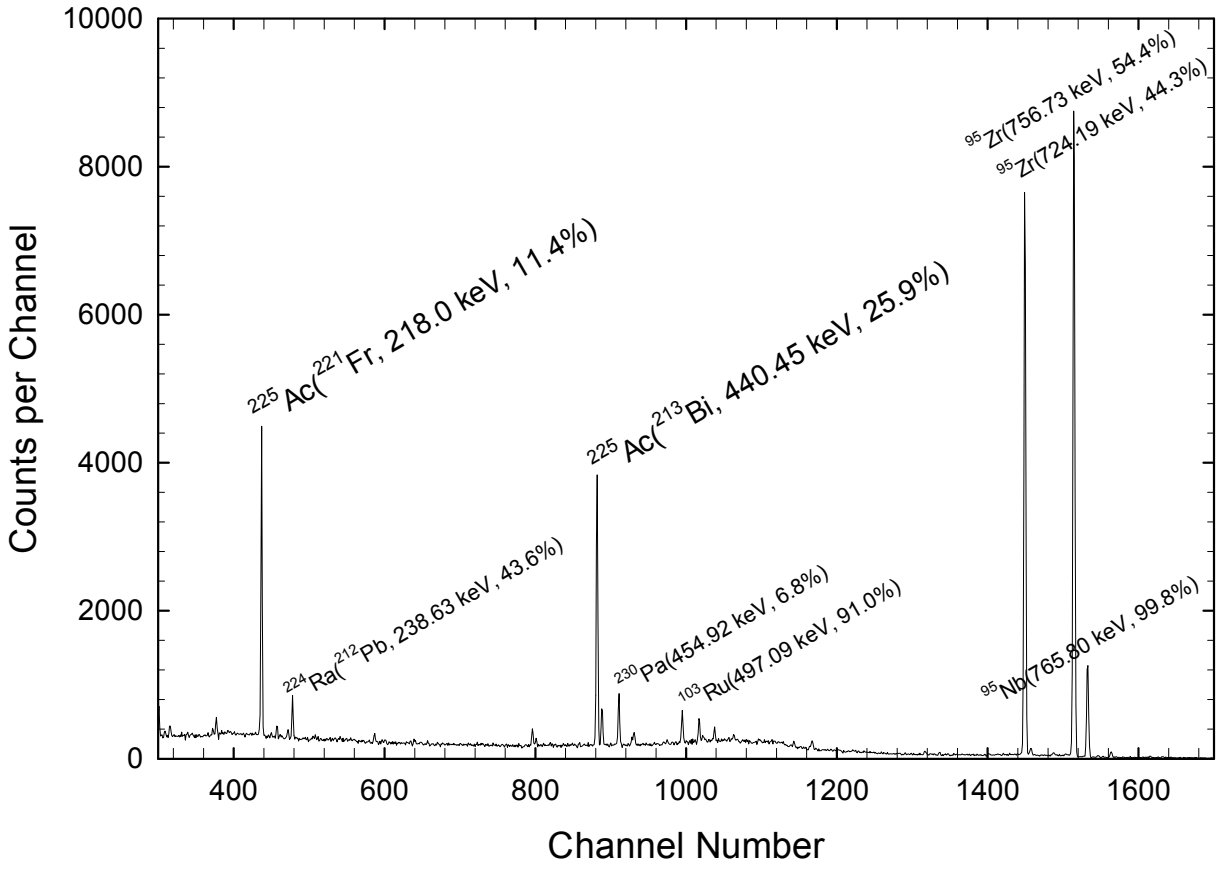

FIG. 6. High-purity germanium γ-ray spectrum of actinium fraction from the thin target experiment showing ^{225}Ac produced from α-decay of ^{229}Pa. The γ rays at 218 keV from ^{221}Fr and 440 keV from ^{213}Bi are representative of ^{225}Ac (spectrum collection time = 5 h).

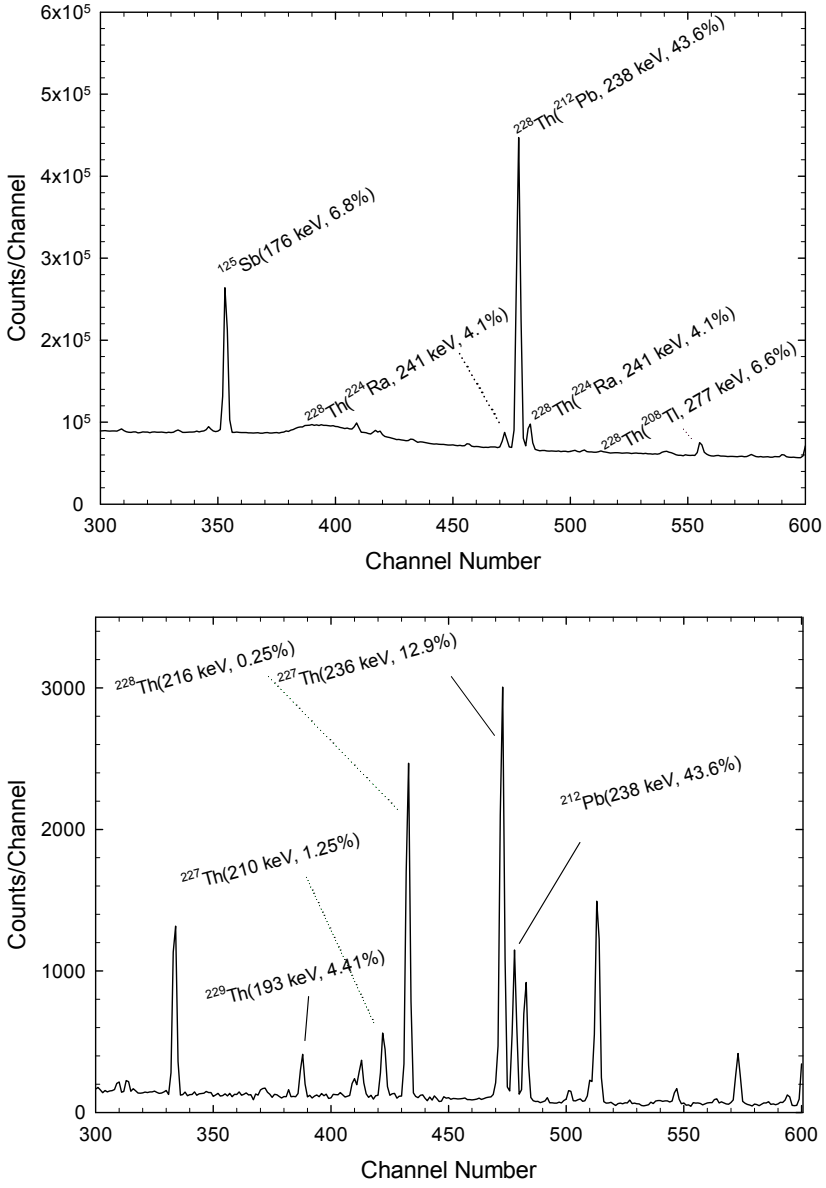

FIG. 7. γ-ray spectra of the purified Th fractions from the thick target at 6 months post EOB; a) before ^{212}Pb removal, and b) after removal of >99% of ^{212}Pb. (a) the 193.52 keV γ ray from the decay of ^{229}Th is not visible due to the Compton continuum generated by γ-ray emissions from ^{228}Th decay daughters (spectrum collection time =15 h). (b) the 193.52 keV γ ray from the decay of ^{229}Th is only visible but only for a short time until ^{228}Th decay daughters grow into equilibrium with ^{228}Th (spectrum collection time = 5 h).

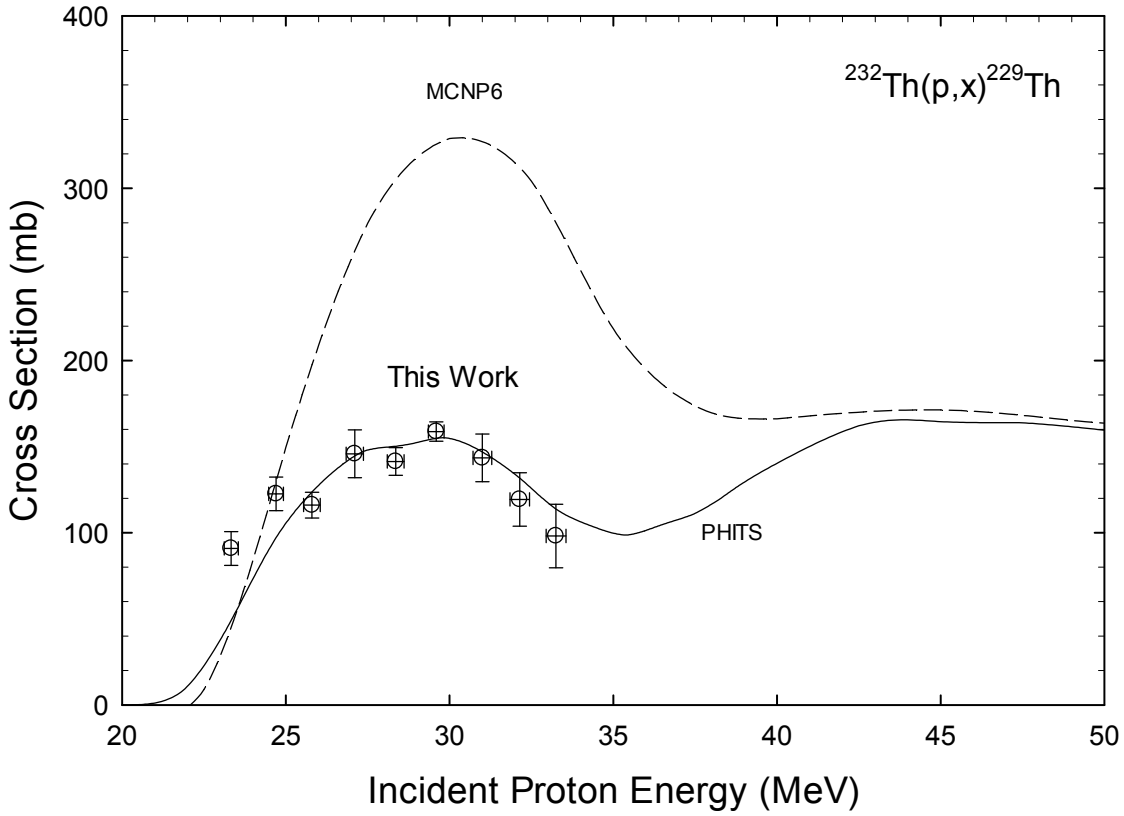

FIG. 8. A comparison of the experimental (data points) and theoretical PHITS (solid line) and MCNP6 (dashed line) excitation functions for the cumulative ^{232}Th(p,x)^{229}Th reaction.

TABLE I. ^{229}Th Production reactions. Threshold energies were calculated from systematics using nuclide masses and conservation of momentum [51].

Reaction	Threshold (MeV)	Coulomb barrier on exit channel (MeV)
^{232}Th(p,nt)^{229}Th	9.9	14.2
^{232}Th(p,2nd)^{229}Th	16.2	14.6
^{232}Th(p,3np)^{229}Th	18.4	15.1
^{232}Th(p,4n)^{229}Pa(EC, $t_{1/2}$ = 1.5 d)^{229}Th	19.5	0
^{232}Th(p,α)^{229}Ac(β^-, $t_{1/2}$ = 62.7 min)^{229}Th	0	27.9
^{232}Th(p,pt)^{229}Ac(β^-, $t_{1/2}$ = 62.7 min)^{229}Th	10.2	29.4
^{232}Th(p,n^{3}He)^{229}Ac(β^-, $t_{1/2}$ = 62.7 min)^{229}Th	11.0	28.5
^{232}Th(p,2d)^{229}Ac(β^-, $t_{1/2}$ = 62.7 min)^{229}Th	14.3	29.1
^{232}Th(p,npd)^{229}Ac(β^-, $t_{1/2}$ = 62.7 min)^{229}Th	16.5	29.7
^{232}Th(p,2n2p)^{229}Ac(β^-, $t_{1/2}$ = 62.7 min)^{229}Th	18.8	30.2
^{232}Th(p,p^{3}He)^{229}Ra(β^-, $t_{1/2}$ = 4.0 min)^{229}Ac(β, $t_{1/2}$ = 62.7 min)^{229}Th	12.1	43.6
^{232}Th(p,2pd)^{229}Ra(β^-, $t_{1/2}$ = 4.0 min)^{229}Ac(β, $t_{1/2}$ = 62.7 min)^{229}Th	17.6	44.8
^{232}Th(p,3pn)^{229}Ra(β^-, $t_{1/2}$ = 4.0 min)^{229}Ac(β, $t_{1/2}$ = 62.7 min)^{229}Th	19.9	45.3

TABLE II. Experimentally evaluated thin target ^{232}Th(p,xn)Pa reaction cross sections.

Incident proton energy (MeV)	Cross section (mb)			
	^{232}Th(p,n)^{232}Pa	^{232}Th(p,3n)^{230}Pa	^{232}Th(p,4n)^{229}Pa	^{232}Th(p,5n)^{228}Pa
13.0 ± 0.8	12.3 ± 0.8	3.4 ± 0.5	—	—
17.1 ± 0.6	17.3 ± 1.3	113.4 ± 7.5	—	—
21.2 ± 0.5	15.7 ± 1.1	372 ± 20	—	—
24.8 ± 0.6	14.7 ± 1.0	176 ± 12	86.0 ± 8.2	—
25.0 ± 0.4	—	171 ± 11	—	2.3 ± 0.5
27.2 ± 0.5	13.6 ± 1.2	85.9 ± 6.3	145 ± 13	3.7 ± 0.3
29.6 ± 0.5	13.0 ± 1.0	59.4 ± 4.3	—	3.8 ± 0.3
29.8 ± 0.2	13.1 ± 1.0	59.8 ± 4.5	162 ± 14	3.9 ± 0.5
31.9 ± 0.4	12.0 ± 0.9	47.3 ± 3.7	106 ± 10	13.0 ± 0.9
34.0 ± 0.5	10.4 ± 0.8	38.5 ± 3.1	64.9 ± 8.5	34.6 ± 2.4
36.0 ± 0.3	10.2 ± 0.8	25.6 ± 2.3	26.9 ± 3.5	60.3 ± 4.1
38.0 ± 0.3	10.6 ± 0.8	24.6 ± 2.4	—	78.8 ± 5.4
39.9 ± 0.2	9.7 ± 0.8	17.4 ± 2.4	8.0 ± 1.1	66.9 ± 4.6

TABLE III. Measured half-life of ^{229}Pa.

Experiment No.	Incident proton energy (MeV)	γ ray used (keV)	Half-life (day)	Error (day)
1	31.9 ± 0.4	117.2	1.83	0.05
		119.0	1.49	0.02
2	29.6 ± 0.5	117.2	2.08	0.06
		119.0	1.60	0.02
3	27.2 ± 0.5	117.2	1.66	0.05
		119.0	1.47	0.02
4	24.8 ± 0.6	117.2	1.78	0.10
		119.0	1.43	0.03
	Weighted average[a], μ'	—	1.55	0.01

[a] Error associated with individual value was used as the weighing factor.

TABLE IV. Experimentally evaluated thick target $^{232}Th(p,x)^{229}Th$ reaction cross sections.

Incident proton energy (MeV)	Cross section (mb)
33.3 ± 0.3	98 ± 18
32.1 ± 0.3	119 ± 16
31.0 ± 0.3	143 ± 14
29.6 ± 0.2	159 ± 6[a]
28.4 ± 0.3	141 ± 8[a]
27.1 ± 0.3	146 ± 14[a]
25.8 ± 0.3	116 ± 8[a]
24.7 ± 0.2	123 ± 10
23.3 ± 0.2	91 ± 10

[a] Weighted average of two independent irradiations with the uncertainty of each individual value used as the weighing factor.